We are IntechOpen, the world's leading publisher of Open Access books Built by scientists, for scientists

4,800
Open access books available

122,000
International authors and editors

135M
Downloads

Our authors are among the

154
Countries delivered to

TOP 1%
most cited scientists

12.2%
Contributors from top 500 universities

CLARIVATE ANALYTICS BOOK CITATION INDEX INDEXED

WEB OF SCIENCE™

Selection of our books indexed in the Book Citation Index in Web of Science™ Core Collection (BKCI)

Interested in publishing with us?
Contact book.department@intechopen.com

Numbers displayed above are based on latest data collected.
For more information visit www.intechopen.com

3

Stiffness Enhancement and Motion Control of a 6-DOF Wire-driven Parallel Manipulator with Redundant Actuations for Wind Tunnels

Xin Liu, Yuanying Qiu and Xuechao Duan
Xidian University
P.R.China

1. Introduction

As is well known, a wire-driven parallel manipulator is a manipulator whose end-effector is driven by a number of cables instead of rigid links. It shows several promising advantages over its rigid-link counterpart, such as simple light-weight mechanical structure, low moment inertia, large reachable workspace and high-speed motion. In the 1980s, the National Institute of Standards and Technology (NIST) in America invented a wire-driven parallel manipulator named RoboCrane for shipyards (Albus et al, 1993). So far, wire-driven parallel manipulators have been applied in load lifting, industrial machining, virtual reality and astronomic observation (Dekker et al, 2006; Ning et al, 2006; Ma & Diao, 2005). Because of the advantages and unique features of wires, wire-driven parallel manipulators have attracted a great attention in robotics literature. The first general classification was given by Ming and Higuchi (Ming and Higuchi, 1994). Based on the number of wires (m) and the number of degrees of freedom (n), wire-driven parallel manipulators were classified into three categories, i.e. the incompletely restrained positioning mechanisms ($m<n+1$), the completely restrained positioning mechanisms ($m=n+1$) and the redundantly restrained positioning mechanisms ($m>n+1$). Yamamoto *et al.* presented basic dynamics equations and a feedback control method based on exact linearization for the incompletely restrained positioning mechanisms (Yamamoto et al, 2004). Hithoshi *et al.* studied a robust PD control using adaptive compensation for translational wire-driven parallel manipulators of a completely restrained type (Hithoshi et al, 2007). Zi Bin *et al.* developed a fuzzy plus proportional-integral control method for the cable-cabin mechanism of 500m aperture spherical radio telescope (Zi et al, 2008). Yu Kun considered active stiffness control schemes as optimization problem with different criteria for redundantly restrained positioning mechanisms (Yu, 2008). In essence, a wire-driven parallel manipulator can be considered as a complex, time-varying, strong-coupled, multiple input and multiple output, and nonlinear system. Since the wires can only pull and not push on the platform, dynamics and control are key issues for high-precision motion of wire-driven parallel manipulators.

Wind tunnel tests of aircraft models are widely utilized to investigate the potential flight dynamics and aerodynamic characteristics of aircrafts at their early developing stage. Wire-driven parallel manipulators have been introduced to wind tunnels as flexible suspension systems of aircraft models in recent years (Liu et al, 2004). The posture of the scale model corresponding to the stream line of airflows can be adjusted by controlling the length of

wires to implement the six degree-of-freedom free flight motion. The aerodynamic forces exerted on the scale model can be calculated by measuring the tension of each wire. Comparing with traditional frame suspension systems, wire-driven parallel manipulators for wind tunnels have advantages in less aerodynamic interference and high precision of the test results. Preliminary achievements have been made in the Suspension ACtive pour Soufflerie (SACSO) project about the wire-driven parallel suspension system in low wind tunnels sponsored by Office National d'Études et de Recherches Aérospatiales (ONERA). The achievements include architecture design, workspace computation, force control and build-up of a prototype of the wire-driven parallel manipulator (Lafourcade, 2004). Zheng Yaqing et al. have developed some fundamental theoretical research work on workspace, wire tension distribution, stiffness, kinematics and control of the manipulators. Because of weak stiffness of wires, the aircraft model would deviate from the planned trajectory when it is in the streamline flow. The trajectory errors have significant effect on the force and moment measurement. Hence one challenging issue is to accurately implement the attitude control for wire-driven parallel manipulators in wind tunnels.

The flexible suspension system in wind tunnels proposed by Zheng, which can be viewed as a six degree-of-freedom eight wires driven parallel manipulator, is investigated in this paper (Zheng, 2004). In order to decrease the trajectory errors and improve the measurement precision, it is necessary to enhance stiffness of the flexible suspension system. In case of wire-driven parallel manipulators with redundant actuations, the stiffness of the manipulators have been researched by Yu (Yu, 2008) and Saeed Behzadipou (Behzadipour & Khajepour, 2006) respectively, based on the stiffness definition and the equivalent spring model. In this paper, an analytic expression of the stiffness of the flexible suspension system in wind tunnels is derived by using the differential transformation principle. In order to hurdle a low rigidity and poor positioning accuracy caused by the minimum wire tension solution, an optimal tension distribution method is applied for the enhancement of stiffness in lift, along-wind and pitching directions. The method resolves the uncertainty of wire tensions of the suspension system.

The motion control of the flexible suspension system in wind tunnels can be realized either in end-effector space or in joint space. The pose of the aircraft model must be measured in real time during the former control process. Measuring the pose of the aircraft model in wind tunnels is rather challenging, because the cross section of wind tunnels is limited and the existence of equipments disturbs air flows. Moreover, it is not desirable to obtain the pose of the aircraft model using direct kinematics, because of lots of time required by complicated calculation. Hence, a computed torque controller in joint space is employed for the flexible suspension system in wind tunnels. A dynamics compensation is introduced to a conventional proportional differential controller, so a modified proportional differential control strategy in the wire length coordinates is developed based on stiffness enhancement.

2. System description

Figure 1 shows the flexible suspension system driven by eight wires. Each wire is attached to the aircraft model at one end, and threads the pulleys mounted to the wind tunnel and winds around an actuated reel at the other end. The actuated reels allow the control of the pose of the aircraft model by controlling the length of their respective wires. The aerodynamic loads on the aircraft model can be calculated through measuring the wire tension by strain gages.

Fig. 1. The flexible suspension system for wind tunnel

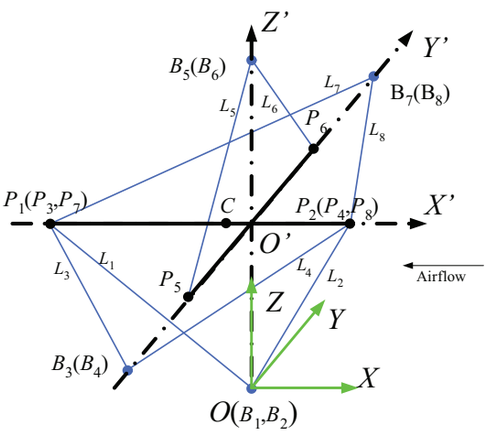

Fig. 2. Geometric definition of the suspension system

All geometric quantities are shown in Fig. 2. *OXYZ* and *O′X′Y′Z′* are coordinate frames attached to the wind tunnel and the aircraft model, respectively. *C* is the center of gravity of the aircraft model. The point where the i^{th} wire leaves the reel is denoted by B_i, and the connecting point on the aircraft model is denoted by P_i. The rotation matrix of the *O′X′Y′Z′* with respect to *OXYZ* is represented by

$$
\begin{aligned}
{}^{o}\boldsymbol{R}_{o'} &= rot(z,\psi)rot(y,\beta)rot(x,\phi) \\
&= \begin{bmatrix} \cos\psi\cos\beta & \cos\psi\sin\beta\sin\phi-\sin\psi\cos\phi & \cos\psi\sin\beta\cos\phi+\sin\psi\sin\phi \\ \sin\psi\cos\beta & \sin\psi\sin\beta\sin\phi+\cos\psi\cos\phi & \sin\psi\sin\beta\cos\phi-\cos\psi\sin\phi \\ -\sin\beta & \cos\beta\sin\phi & \cos\beta\cos\phi \end{bmatrix}
\end{aligned} \tag{1}
$$

where ϕ, β and ψ are the roll, pitch and yaw angles of the aircraft model respectively. The length of the i^{th} wire is expressed by

$$
l_i = \left\| {}^{o}\boldsymbol{L}_i \right\|_2 = \sqrt{({}^{o}\boldsymbol{B}_i - {}^{o}\boldsymbol{P}_{o'} - {}^{o}\boldsymbol{R}_{o'}{}^{o'}\boldsymbol{P}_i)^{\mathrm{T}}({}^{o}\boldsymbol{B}_i - {}^{o}\boldsymbol{P}_{o'} - {}^{o}\boldsymbol{R}_{o'}{}^{o'}\boldsymbol{P}_i)} \quad \text{for } i=1,2,\ldots,8 \tag{2}
$$

where ${}^{o}\boldsymbol{L}_i = {}^{o}\boldsymbol{B}_i - {}^{o}\boldsymbol{P}_{o'} - {}^{o}\boldsymbol{R}_{o'}{}^{o'}\boldsymbol{P}_i$,

${}^{o}\boldsymbol{P}_{o'} = [{}^{o}x_{o'}\ {}^{o}y_{o'}\ {}^{o}z_{o'}]^{\mathrm{T}}$ is the position vector of the mobile frame's origin,

${}^{o'}\boldsymbol{P}_i = [{}^{o'}x_{p_i}\ {}^{o'}y_{p_i}\ {}^{o'}z_{p_i}]^{\mathrm{T}}$ is the position vector of point P_i in the mobile frame $O'X'Y'Z'$,

${}^{o}\boldsymbol{B}_i = [{}^{o}x_{B_i}\ {}^{o}y_{B_i}\ {}^{o}z_{B_i}]^{\mathrm{T}}$ is the position vector of point B_i in the fixed frame $OXYZ$.

Differentiating Eq.(2) with respect to time, and then assembling the eight resulting equations into matrix form, we obtain

$$\dot{\boldsymbol{l}} = -\boldsymbol{J}^{\mathrm{T}}\dot{\boldsymbol{X}} \tag{3}$$

where $\boldsymbol{l} = [l_1\ l_2\ \cdots\ l_8]^{\mathrm{T}}$ is the wire-length vector,

$\boldsymbol{X} = [{}^{o}x_{o'}\ {}^{o}y_{o'}\ {}^{o}z_{o'}\ \ \phi\ \ \beta\ \ \psi]^{\mathrm{T}}$ is the posture vector of the aircraft model,

$\boldsymbol{J} = \begin{bmatrix} {}^{o}\boldsymbol{u}_1 & {}^{o}\boldsymbol{u}_2 & \cdots & {}^{o}\boldsymbol{u}_8 \\ ({}^{o}\boldsymbol{R}_{o'}{}^{o'}\boldsymbol{P}_1)\times {}^{o}\boldsymbol{u}_1 & ({}^{o}\boldsymbol{R}_{o'}{}^{o'}\boldsymbol{P}_2)\times {}^{o}\boldsymbol{u}_2 & \cdots & ({}^{o}\boldsymbol{R}_{o'}{}^{o'}\boldsymbol{P}_8)\times {}^{o}\boldsymbol{u}_8 \end{bmatrix} \in \mathbf{R}^{6\times 8}$ is a pose-dependent matrix,

${}^{o}\boldsymbol{u}_i = {}^{o}\boldsymbol{L}_i \Big/ \left\| {}^{o}\boldsymbol{L}_i \right\|_2$ is the unit vector along the i^{th} wire.

The equation of static equilibrium can be written as

$$\boldsymbol{J}\boldsymbol{T} + \boldsymbol{F} = \boldsymbol{0} \tag{4}$$

where $\boldsymbol{T} = [t_1\ t_2\ \cdots\ t_8]^{\mathrm{T}}$ is the wire tension vector, $\boldsymbol{F} = \begin{bmatrix} \boldsymbol{F}_R \\ \boldsymbol{M}_R \end{bmatrix}$ summarizes all other force and torques acting on the aircraft model.

3. Analytic stiffness

The influence of the wire tension on stiffness of the flexible suspension system is investigated, and an analytic expression of the stiffness is derived from the differential transformation principle. When an infinitesimal wrench $\partial\boldsymbol{F}$ is applied to the aircraft model, the posture of the aircraft model changes by an infinitesimal deflection $\partial\boldsymbol{X}$. The Stiffness matrix $\boldsymbol{K}$ of the suspension system is

$$\boldsymbol{K} = \frac{\partial \boldsymbol{F}}{\partial \boldsymbol{X}} = -\frac{\partial \boldsymbol{J}}{\partial \boldsymbol{X}}\boldsymbol{T} - \boldsymbol{J}\frac{\partial \boldsymbol{T}}{\partial \boldsymbol{X}} \tag{5}$$

For the first term in the equation (5), $\partial\boldsymbol{J}$ can be expressed by the product of an infinitesimal deflection $\partial\boldsymbol{X}$ and a three-dimensional matrix which excludes $\partial\boldsymbol{X}$. Assuming the matrix $\boldsymbol{H}$ is equal to $\dfrac{\partial \boldsymbol{J}}{\partial \boldsymbol{X}}$, we obtain

$$\begin{cases} \boldsymbol{H} = \begin{bmatrix} \boldsymbol{H}_1 & \boldsymbol{H}_2 & \cdots & \boldsymbol{H}_8 \end{bmatrix} \in \mathbf{R}^{6\times 6\times 8} \\ \boldsymbol{H}_i = \dfrac{1}{l_i}\begin{bmatrix} -\boldsymbol{I} & {}^{o}\boldsymbol{P}_i\times \\ -({}^{o}\boldsymbol{R}_{o'}{}^{o'}\boldsymbol{P}_i)\times & [{}^{o}\boldsymbol{L}_i\times][({}^{o}\boldsymbol{R}_{o'}{}^{o'}\boldsymbol{P}_i)\times] - [({}^{o}\boldsymbol{R}_{o'}{}^{o'}\boldsymbol{P}_i)\times][{}^{o}\boldsymbol{P}_i\times] \end{bmatrix} \in \mathbf{R}^{6\times 6} \end{cases} \tag{6}$$

where $(\ )\times$ is the operator representing cross product.

As for the second term in the equation (5), we have

$$-\boldsymbol{J}\frac{\partial \boldsymbol{T}}{\partial \boldsymbol{X}} = -\boldsymbol{J}\frac{\partial \boldsymbol{T}}{\partial \boldsymbol{L}}\cdot\frac{\partial \boldsymbol{L}}{\partial \boldsymbol{X}} = k^{'}\boldsymbol{J}diag(\frac{1}{l_{0i}})\boldsymbol{J}^{\mathrm{T}} = k^{'}\boldsymbol{J}diag(l_i^{-1}(1+k^{'-1}t_i))\boldsymbol{J}^{\mathrm{T}} \quad \text{for } i=1,\ldots,8 \tag{7}$$

where $k^{'} = EA$,
E is Young's modulus of a wire,
A is the cross section area of a wire,
l_i is the currently measured length of the i^{th} wire,
l_{0i} is the original length of the i^{th} wire.

It is pointed out that the contribution of $k^{'-1}t_i$ to the stiffness of the suspension system can be neglected because it is much less than one. The stiffness of the suspension system consists of two parts, while the first one is mainly influenced by the wire tension and the other one depends on geometrical arrangement of the wires and posture of the aircraft model. Supposing the external wrench $\boldsymbol{F}$ acted on the aircraft model is known, the wire tension in equation (4) can be written as

$$\boldsymbol{T} = -\boldsymbol{J}^{+}\boldsymbol{F} + \boldsymbol{Null}(\boldsymbol{J})\boldsymbol{\lambda} \tag{8}$$

where $\boldsymbol{J}^{+} = \boldsymbol{J}^{\mathrm{T}}(\boldsymbol{J}\boldsymbol{J}^{\mathrm{T}})^{-1} \in \mathbf{R}^{8\times 6}$ is the Moore-Penrose inverse of matrix $\boldsymbol{J}$, $\boldsymbol{Null}(\boldsymbol{J}) \in \mathbf{R}^{8\times 2}$ is a matrix whose columns form a basis for the null-space of matrix $\boldsymbol{J}$, $\boldsymbol{\lambda} = [\lambda_1\ \lambda_2]^{\mathrm{T}} \in \mathbf{R}^{2\times 1}$ is a column vector of two arbitrary real numbers.
The solution in equation (8) consists of two parts: the first one is the term $-\boldsymbol{J}^{+}\boldsymbol{F}$, which represents the minimum-norm solution that minimizes the 2-norm $\|\boldsymbol{T}\|$. The second part $Null(\boldsymbol{J})\boldsymbol{\lambda}$ is an arbitrary vector in the mull-space of matrix $\boldsymbol{J}$ and, affects the distribution of the wire tension without affecting the force and moment at the aircraft model. Equation (5) can be rewritten as

$$\boldsymbol{K} \approx \boldsymbol{H}(\boldsymbol{J}^{+}\boldsymbol{F} - Null(\boldsymbol{J})\boldsymbol{\lambda}) + k^{'}\boldsymbol{J}diag(\frac{1}{l_i})\boldsymbol{J}^{\mathrm{T}} \tag{9}$$

It is clearly seen that the wire tension can be changed by adjusting the two elements of the column vector $\boldsymbol{\lambda}$, and then the wire tension can make an impact on the stiffness of the system.

4. Dynamic models

4.1 Dynamic Model of the aircraft model

By using Newton-Euler's laws, the motion equations of the aircraft model can be written in the following form

$$\begin{cases} m\ddot{\boldsymbol{x}} + m\dot{\boldsymbol{\omega}}\times {}^{o}\boldsymbol{C} + m\boldsymbol{\omega}\times(\boldsymbol{\omega}\times {}^{o}\boldsymbol{C}) = \sum_{i=1}^{8} {}^{o}\boldsymbol{u}_i t_i + m\boldsymbol{g} + \boldsymbol{F}_e \\ m\,{}^{o}\boldsymbol{C}\times\ddot{\boldsymbol{x}} + \boldsymbol{I}\dot{\boldsymbol{\omega}} + m(\boldsymbol{\omega}\times {}^{o}\boldsymbol{C})\times\dot{\boldsymbol{x}} + \boldsymbol{\omega}\times(\boldsymbol{I}\boldsymbol{\omega}) = \sum_{i=1}^{8} {}^{o}\boldsymbol{P}_i\times {}^{o}\boldsymbol{u}_i t_i + {}^{o}\boldsymbol{C}\times m\boldsymbol{g} + \boldsymbol{M}_e \end{cases} \tag{10}$$

where $\dot{\boldsymbol{x}} = [{}^{o}\dot{x}_{o'}\ {}^{o}\dot{y}_{o'}\ {}^{o}\dot{z}_{o'}]^{\mathrm{T}}$ represents the linear velocity of the reference point O' of the aircraft model,

$\boldsymbol{\omega} = [\dot{\phi}\ \dot{\beta}\ \dot{\psi}]^{\mathrm{T}}$ is the angular velocity of the aircraft model,

m is the mass of the aircraft model,

$\boldsymbol{g} = [0\ 0\ g]^{\mathrm{T}}$ and scalar g is the gravity acceleration,

${}^{o}\boldsymbol{C} = {}^{o}\boldsymbol{R}_{o'}\,{}^{o'}\boldsymbol{C}$ and ${}^{o'}\boldsymbol{C}$ is position vector of the center of gravity of the aircraft model in the mobile frame $O'X'Y'Z'$,

$\boldsymbol{I} = {}^{o}\boldsymbol{R}_{o'}\boldsymbol{I}_{o'}\,{}^{o}\boldsymbol{R}_{o'}^{\mathrm{T}}$ and $\boldsymbol{I}_{o'} = \begin{bmatrix} I_{X'X'} & -I_{X'Y'} & -I_{X'Z'} \\ -I_{Y'X'} & I_{Y'Y'} & -I_{Y'Z'} \\ -I_{Z'X'} & -I_{Z'Y'} & I_{Z'Z'} \end{bmatrix}$ is the inertia tensor of the aircraft model in the mobile frame $O'X'Y'Z'$,

$\boldsymbol{F}_e$ and $\boldsymbol{M}_e$ are the force and moment exerted by aerodynamic load on the aircraft model.

Equation (10) can be re-written into a compact form as

$$\boldsymbol{M}(\boldsymbol{X})\ddot{\boldsymbol{X}} + \boldsymbol{N}(\boldsymbol{X}, \dot{\boldsymbol{X}})\dot{\boldsymbol{X}} = \boldsymbol{W}_e + \boldsymbol{W}_g + \boldsymbol{J}\boldsymbol{T} \tag{11}$$

where $\boldsymbol{M} = \begin{bmatrix} m\boldsymbol{1} & -m\,{}^{o}\boldsymbol{C}\times \\ m\,{}^{o}\boldsymbol{C}\times & \boldsymbol{I} \end{bmatrix}$ and $\boldsymbol{I} \in \mathbf{R}^{3\times 3}$ is the identity matrix,

$\boldsymbol{N} = \begin{bmatrix} \boldsymbol{0} & -m(\boldsymbol{\omega}\times {}^{o}\boldsymbol{C})\times \\ m(\boldsymbol{\omega}\times {}^{o}\boldsymbol{C})\times & -\boldsymbol{I}\boldsymbol{\omega} \end{bmatrix}$ and $\boldsymbol{0} \in \mathbf{R}^{3\times 3}$ is the zero matrix,

$\boldsymbol{W}_e = \begin{bmatrix} \boldsymbol{F}_e \\ \boldsymbol{M}_e \end{bmatrix}$ is the aerodynamic wrench acted on the aircraft model,

$\boldsymbol{W}_g = \begin{bmatrix} m\boldsymbol{g} \\ {}^{o}\boldsymbol{C}\times m\boldsymbol{g} \end{bmatrix}$ is the gravity wrench exerted on the reference point O' of the aircraft model,

$\dot{\boldsymbol{X}} = \begin{bmatrix} \dot{\boldsymbol{x}} \\ \boldsymbol{\omega} \end{bmatrix}$ is the velocity vector of the aircraft model.

4.2 Dynamic model of the drive units

A drive unit is composed of a motor, a gear reducer and a winch. The dynamic equation of the drive units is given as follows

$$\boldsymbol{A}\ddot{\boldsymbol{\theta}} + \boldsymbol{C}\dot{\boldsymbol{\theta}} + \boldsymbol{r}\boldsymbol{T} = \boldsymbol{\tau} \tag{12}$$

with $\boldsymbol{A} = diag(a_1, a_2, \cdots a_8)$, $a_i = a_{ai} + \dfrac{a_{wi}}{n^2}$,

$\boldsymbol{C} = diag(c_1, c_2, \cdots c_8)$, $c_i = c_{ai} + \dfrac{c_{wi}}{n}$,

$\boldsymbol{r} = diag(r_1, r_2, \cdots r_8)$, $r_i = \dfrac{r_{wi}}{n}$,

$\boldsymbol{\theta} = [\theta_1\ \theta_2\ \cdots\ \theta_8]^{\mathrm{T}}$,

$\boldsymbol{\tau} = [\tau_1 \ \tau_2 \ \cdots \ \tau_8]^{\mathrm{T}}$,

where a_{ai}, c_{ai} denote the moment of inertia and the vicious friction coefficient of the i^{th} motor,

a_{wi}, c_{wi} denote the moment of inertia and the vicious friction coefficient of the i^{th} reducer and winch,

r_{wi} is the radius of the i^{th} winch,

n is the reduced ratio of each gear reducer,

θ_i is the rotational angle of the i^{th} motor,

τ_i is the output torque of the i^{th} motor.

4.3 The elastic model of the wires

The relationship between the change of the wire length and the rotational angles of the motors is

$$\boldsymbol{\theta} = \boldsymbol{r}^{-1}\begin{Bmatrix} \left\| {}^{o}\boldsymbol{B}_1 \right\|_2 - \left\| {}^{o}\boldsymbol{B}_1 - {}^{o}\boldsymbol{P}_{o'} - {}^{o}\boldsymbol{R}_{o'}\,{}^{o'}\boldsymbol{P}_1 \right\|_2 \\ \vdots \\ \left\| {}^{o}\boldsymbol{B}_8 \right\|_2 - \left\| {}^{o}\boldsymbol{B}_8 - {}^{o}\boldsymbol{P}_{o'} - {}^{o}\boldsymbol{R}_{o'}\,{}^{o'}\boldsymbol{P}_8 \right\|_2 \end{Bmatrix} \tag{13}$$

Successive time derivatives of equation (13) yield

$$\dot{\boldsymbol{\theta}} = \frac{\partial \boldsymbol{\theta}}{\partial \boldsymbol{X}}\dot{\boldsymbol{X}} = \frac{\partial \boldsymbol{\theta}}{\partial \boldsymbol{l}}\frac{\partial \boldsymbol{l}}{\partial \boldsymbol{X}}\dot{\boldsymbol{X}} = \boldsymbol{r}^{-1}\boldsymbol{J}^{\mathrm{T}}\dot{\boldsymbol{X}} \tag{14}$$

$$\ddot{\boldsymbol{\theta}} = \boldsymbol{r}^{-1}\dot{\boldsymbol{J}}^{\mathrm{T}}\dot{\boldsymbol{X}} + \boldsymbol{r}^{-1}\boldsymbol{J}^{\mathrm{T}}\ddot{\boldsymbol{X}} \tag{15}$$

The elasticity of the wires must be taken into account in order to increase motion control accuracy. The longitudinal deformation of a wire can be given by

$$\Delta l_i = \frac{t_i l_{0i}}{EA} \tag{16}$$

Then the stiffness of a wire is $k_i = \dfrac{EA}{l_{0i}} = \dfrac{EA}{l_i(1-\Delta l_i / l_i)}$. To summarize, Equations (11), (12), (13), (14) and (15) represent the dynamic model of the suspension system in wind tunnel.

5. Control scheme

The dynamic model of the flexible suspension system in wind tunnels is a highly-coupled and nonlinear system, and the actuation redundancy makes the system over-restrained. In designing the control scheme, it is necessary to decouple and linearize the dynamic model. A computed torque controller in joint space is employed for the flexible suspension system in wind tunnels. Because the actuation redundancy introduces multiple wire tension solutions, an optimal tension distribution method is applied to obtain certain acceptable solutions. When the air flow passes through the aircraft model in wind tunnel tests, a wind pressure will be exerted on the aircraft model. According to the aerodynamic theory, drag

force in along-wind direction, lift force in crosswind direction and pitching moment are applied on the model under the condition that the wind load is symmetrical. The wind load make the model fail to keep the desired position and orientation. Thus, it is challenging to obtain the accurate mapping relation between the measured value of the aerodynamics and the position and orientation of the craft model. Consequently, it is desired to enhance the stiffness in the three directions by commanding the wire tensions. Further more, by introducing the dynamical compensation on the basis of conventional PD control, the revised feedforward PD control law based on the stiffness enhancement principles. As shown in Fig. 3, the control law consisting of inverse dynamics feedforward and feedback loop is employed to control the driving torque of the actuators.

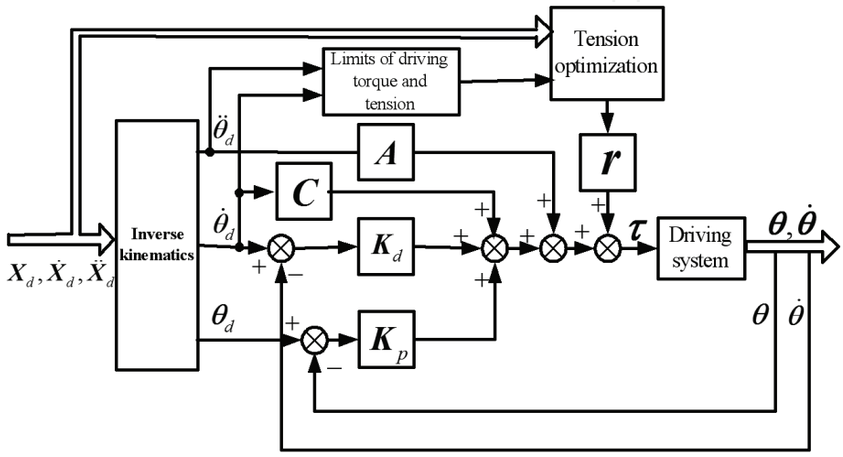

Fig. 3. Control scheme for wire-driven parallel support system for wind tunnels

The revised PD feedforward control law is

$$\boldsymbol{\tau} = \boldsymbol{A}\ddot{\boldsymbol{\theta}}_d + \boldsymbol{C}\dot{\boldsymbol{\theta}}_d + \boldsymbol{r}\boldsymbol{T}_d + \boldsymbol{K}_p(\boldsymbol{\theta}_d - \boldsymbol{\theta}) + \boldsymbol{K}_d(\dot{\boldsymbol{\theta}}_d - \dot{\boldsymbol{\theta}}) \tag{17}$$

where, $\boldsymbol{K}_P$, $\boldsymbol{K}_d$ are feedback gain matrices. $\boldsymbol{T}_d$ is the desired tension. Error $\boldsymbol{e} = \boldsymbol{\theta} - \boldsymbol{\theta}_d$. If the desired angular velocity $\dot{\boldsymbol{\theta}}_d$, angular acceleration $\ddot{\boldsymbol{\theta}}_d$ and tension $\boldsymbol{T}_d$ are all boundary values, Eq.(17) can make $\boldsymbol{e}$ and $\dot{\boldsymbol{e}}$ exponentially converge to the closed sphere of radius r_i. Provided the desired trajectory $\boldsymbol{X}_\mathrm{d}$ of the aircraft model, the desired angle, angular velocity and angular acceleration of the driving motors can be solved for by using inverse kinematics and the elastic deformation Eq.(16).

$$\boldsymbol{T}_d = \bar{\boldsymbol{T}}_d + \boldsymbol{Null}(\boldsymbol{J})\boldsymbol{\lambda} \tag{18}$$

$$\bar{\boldsymbol{T}}_d = \boldsymbol{J}^{+}(\boldsymbol{M}(\boldsymbol{X}_d)\ddot{\boldsymbol{X}}_d + \boldsymbol{N}(\boldsymbol{X}_d, \dot{\boldsymbol{X}}_d)\dot{\boldsymbol{X}}_d - \boldsymbol{W}_g) \tag{19}$$

where $\bar{\boldsymbol{T}}_d$ is the minimal norm solution. ***Null*** is the null space vector. The restrictions for single wire and the torque of the motors are $\tau_{\max} \geq \tau_i \geq \tau_{\min}$, where $t_{\max}$ is the maximum permissive tension of the wire, and $t_{\min}$ is the minimum tension of the wire in case of the pseudo drag. $\tau_{\max}$ and $\tau_{\min}$ are the maximum and minimum output torque, respectively. Further, we can obtain

$$\boldsymbol{\varphi} \geq \boldsymbol{T} \geq \boldsymbol{\eta} \tag{20}$$

where, $\varphi_i = \min\left\{t_{\max}, (\tau_{\max} - a_i\ddot{\theta}_{id} - c_i\dot{\theta}_{id})/r_i\right\}$, $\eta_i = \max\left\{t_{\min}, (\tau_{\min} - a_i\ddot{\theta}_{id} - c_i\dot{\theta}_{id})/r_i\right\}$,

$\boldsymbol{\varphi}=[\varphi_1 \ \cdots \ \varphi_8]^{\mathrm{T}}$, $\boldsymbol{\eta}=[\eta_1 \ \cdots \ \eta_8]^{\mathrm{T}}$.

For redundant driving system, an optimization is needed to solve for the tensions of the wires. Generally, the tension minimization principle is used in the optimization (Müller, 2005). That is to say $\boldsymbol{T}_d^{\mathrm{T}}\boldsymbol{W}\boldsymbol{T}_d$ and $\boldsymbol{W}$ are the summing weights factor matrices. However, since this parallel robot is applied in wind tunnel, the aircraft model tends to deviate from desired position and orientation and results in experimental errors. Consequently, in order to obtain more precise experimental data, it is necessary to enhance the stiffness by adjusting wire tension. Taking account of constrains of the motor output and wire material properties, the objective of the optimization is to maximize the stiffness weight-sum in the three principal directions of forces or torques.

$$\begin{aligned} &\textit{find} \quad \boldsymbol{\lambda} = [\lambda_1 \quad \lambda_2]^{\mathrm{T}} \\ &\max \ \ \mathrm{sum}(K_{XX}{}^{g_1}, K_{ZZ}{}^{g_2}, K_{\beta\beta}{}^{g_3}) \\ &s.t. \quad \boldsymbol{\varphi}(\dot{\boldsymbol{\theta}}_d, \ddot{\boldsymbol{\theta}}_d) - \bar{\boldsymbol{T}}_d \geq \boldsymbol{Null}(\boldsymbol{J})\boldsymbol{\lambda} \geq \boldsymbol{\eta}(\dot{\boldsymbol{\theta}}_d, \ddot{\boldsymbol{\theta}}_d) - \bar{\boldsymbol{T}}_d \end{aligned} \tag{21}$$

Given the desired trajectory of the aircraft model $\boldsymbol{X}_d$, $\bar{\boldsymbol{T}}_d$, $\boldsymbol{\varphi}(\dot{\boldsymbol{\theta}}_d, \ddot{\boldsymbol{\theta}}_d)$ and $\boldsymbol{\eta}(\dot{\boldsymbol{\theta}}_d, \ddot{\boldsymbol{\theta}}_d)$ can be solved from Eq. (19) and (20). The translational stiffness in X direction is $K_{XX} = \boldsymbol{K}_{1,1} = k'\sum_{i=1}^{8}\frac{\boldsymbol{u}_{i,1}^2}{l_i} + \sum_{i=1}^{8} -\frac{1}{l_i}(\bar{\boldsymbol{T}}_{d,i} + \lambda_1\boldsymbol{Null}(\boldsymbol{J})_{i,1} + \lambda_2\boldsymbol{Null}(\boldsymbol{J})_{i,2})$. That in Z direction is $K_{ZZ} = \boldsymbol{K}_{3,3} = k'\sum_{i=1}^{8}\frac{\boldsymbol{u}_{i,3}^2}{l_i} + \sum_{i=1}^{8} -\frac{1}{l_i}(\bar{\boldsymbol{T}}_{d,i} + \lambda_1\boldsymbol{Null}(\boldsymbol{J})_{i,1} + \lambda_2\boldsymbol{Null}(\boldsymbol{J})_{i,2})$. The stiffness in the pitching direction is $K_{\beta\beta} = \boldsymbol{K}_{5,5} = \sum_{i=1}^{8}\frac{([{}^o\boldsymbol{L}_i\times][({}^o\boldsymbol{R}_o, {}^{o'}\boldsymbol{P}_i)\times] - [({}^o\boldsymbol{R}_o, {}^{o'}\boldsymbol{P}_i)\times][{}^o\boldsymbol{P}_i\times])_{2,2}}{l_i}(\bar{\boldsymbol{T}}_{d,i} + \lambda_1\boldsymbol{Null}(\boldsymbol{J})_{i,1} + \lambda_2\boldsymbol{Null}(\boldsymbol{J})_{i,2}) + k'\sum_{i=1}^{8}\frac{({}^o\boldsymbol{P}_i \times {}^o\boldsymbol{u}_i)_2^2}{l_i}$. The subscript indicates the row element of a vector or the element of a matrix. For the dimensionally generalized K_{XX}, K_{ZZ} and $K_{\beta\beta}$, the objective function is derived by weighting sum. And the weight sum factors g_1, g_2 and g_3 are determined according to the desired trajectory and index of the experiment. The optimization objective is the linear function of λ_1 and λ_2, while the constraint function constitutes two-dimensional convex set of λ_1 and λ_2.

For this kind of linear program problem, the simplex search method is generally employed to solve the solution. But the solving course is very time consuming. To improve the computation speed, a new algorithm is designed as follow.

Step 1: Determining the initial solution. There are sixteen linear inequality constrains in Eq.(21). Any three can be picked out and converted into equality constrains. Then the three line equation related to λ_1 and λ_2 from the geometry point of view is obtained. The three intersection points of the three lines can be solved. Then whether the three intersection points

satisfy the rest thirteen inequalities is checked. If so, the three intersection points generate the initial solution by forming a convex combination. If not, another selection is needed.

Step 2: Determining the searching direction. Taking the initial solution obtained in Step 1 as the start point. Along the gradient and negative gradient direction of the objective function forward search step are conducted, respectively. Then the new two candidates are evaluated with respect to the objective function. The direction relating to the better candidate is taken as the searching direction. So, this optimization becomes a one dimensional optimization.

Step 3: Along the searching direction search is conducted forward with larger step until exceeds the feasible region. Then the dichotomy is used between the outer and inner points of the feasible region until the optimal point on the boundary of the feasible region is obtained.

Step 4: In order to maintain the continuity of the wire tension, a judgment of the tension vector is conducted. In which, whether the tension $\boldsymbol{T}_i$ of the current position and orientation and $\boldsymbol{T}_{i\text{-}1}$ of the previous position and orientation satisfy $\left\|\boldsymbol{T}_i - \boldsymbol{T}_{i-1}\right\|_\infty \le \varepsilon$ is judged, where ε is the threshold. If it is satisfied, the optimal solution is obtained. If it is not satisfied, starting with the current solution, along with the positive searching direction the optimization is moved back to the feasible region and the inferior solution is obtained. And the optimization goes to Step 1.

6. Simulated results

In order to validate the proposed algorithm in this research, simulations aiming at the revised PD feedforward controller based on the stiffness enhancement are conducted. Moreover, a comparison between that of a revised PD controller based on tension minimization is carried out.

The position of the joints and pulley of the robot is shown in Table 1. The wire is chosen from reference (Zheng, 2004), which is made of extra strong polyethylene fibre. The diameter $A = 1\text{mm}$ and the Young's modulus is $E = 120\text{GPa}$. The unit stiffness of the wire is $k' = 94247\text{N}$. The maximum elastic tension is $t_{\max} = 1200\text{N}$. The preset minimum pretension is $t_{\min} = 10\text{N}$. The rating output torque of the motors is $\tau_{\max} = 15.8\text{N}\cdot\text{m}$, $\tau_{\min} = -15.8\text{N}\cdot\text{m}$. The equivalent moment of inertia on the shaft of the motors is $7.52\times10^{-4}\,\text{kg}\cdot\text{m}^2$. The equivalent viscosity coefficient on the shaft of the motors is $1.88\times10^{-4}\,\text{N}\cdot\text{m}\cdot\text{s}$. The radius of the wrench is $r_{wi} = 0.04\text{m}$. The ratio of the reducer is 4:1. The scale model is the 1/18 wooden aircraft model referred to in (Liu et al, 2005). The aircraft has a length of 713mm and wing width of 510mm. The height is 107mm and the weight is 10.5N. In the local frame, the inertial tensor is

$$\boldsymbol{I}_{o'} = \begin{bmatrix} 1.0726\times10^{-2} & 0 & -1.8748\times10^{-9} \\ 0 & 2.8409\times10^{-2} & 1.578\times10^{-4} \\ -1.8748\times10^{-9} & 1.578\times10^{-4} & 3.8985\times10^{-2} \end{bmatrix} \text{kg}\cdot\text{m}^2$$

In the experiment, the stable wind with the velocity of 30m/s is applied. Considering the real-time measured data, the equivalent of load force of the wind is generated in MATLAB. The position of the aircraft is ${}^{o}\boldsymbol{P}_{o'} = \begin{pmatrix} 0 & 0 & 420 \end{pmatrix}^{\mathrm{T}}$ mm and its pitch angle varies according to the

following parameter. The desired angle trajectory is $\beta_d = \pi/30 - \omega_\beta t$ and angular velocity is $\omega_\beta = \pi/45$ rad/s , $0 \le t \le 4$s . In order to achieve the precision of the positioning and pitching, the weight factor is $g_1 = 0.3$, $g_2 = 0.3$ and $g_3 = 0.4$. The simulation is conducted employing the fourth order Runge-Kutta method. The sampling time is 0.01s. The PD parameters are determined by both extension critical proportion and manual adjusting method. $\boldsymbol{K}_p = diag(10,10,5.5,5.5,5.5,5.5,5.5,5.5)$, $\boldsymbol{K}_d = diag$ (0.25,0.25,0.15,0.15, 0.15,0.15,0.15,0.15).

Indication	Coordinates(in mm)
${}^{o'}P_1({}^{o'}P_3, {}^{o'}P_7)$	$(-438\ 0\ 0)^T$
${}^{o'}P_2({}^{o'}P_4, {}^{o'}P_8)$	$(275\ 0\ 0)^T$
${}^{o'}P_5$	$(0\ -255\ 0)^T$
${}^{o'}P_6$	$(0\ 255\ 0)^T$
${}^{o'}C$	$(-25\ 0\ 0)^T$
${}^{o}B_1({}^{o}B_2)$	$(0\ 0\ 0)^T$
${}^{o}B_3({}^{o}B_4)$	$(0\ -605\ 420)^T$
${}^{o}B_5({}^{o}B_6)$	$(0\ 0\ 840)^T$
${}^{o}B_7({}^{o}B_8)$	$(0\ 605\ 420)^T$

Table 1. Location of the joints and pulleys

Figs. 4 and 5 show the wire tension based on the stiffness optimization principle and the wind load variation in three directions in the process of adjusting the orientation of the model. Figs 6 and 7 show the wire tension based on the minimum tension principle and the variation of the stiffness in three directions. Fig 8 shows the actual variation curve of the pitch angle in the cases of the two principles. Fig 9 makes a comparison of the positioning error of the aircraft model in *X* and *Z* directions.

As the figures show, the wire tension with the stiffness optimization principle varies evenly. The pitching stiffness $K_{\beta\beta}$ ranges from 8300 to 8700 Nm/rad. The pitch angle error is less than 0.039 rad, and its RMS is 0.0157 rad. The positioning error in *X* direction is less than 0.0111m, and its RMS is 0.0057m. The positioning error is less than 0.013m, and its RMS is 0.0041m.

Under the condition of minimum wire tension principle, the wire tension is small and varies evenly. The pitching stiffness ranges from 7600 to 8000 Nm/rad. The pitching angle error is less than 0.0619 rad, and its RMS is 0.0229rad. The positioning error in *X* direction is less than 0.0185m, and its RMS is 0.0076m. The positioning error in Z direction is less than 0.0178m and the RMS is 0.005m.

Though the wire tension based on optimal stiffness principle tends to be large, compared with that of minimum tension principle the pitching stiffness increases from about 7600-8000 Nm/rad to about 8300 – 8700Nm/rad. The RMS of the pitch angle error decreases by 31.44%. The RMS of the positioning error in X direction decreases by 25%, and that in *Z* direction decreases by 18. The control precision has been improved drastically.

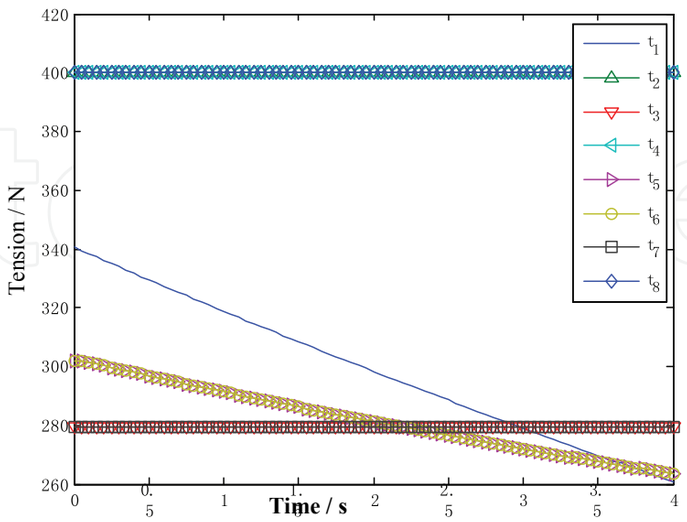

Fig. 4. Optimum tension distribution based on the stiffness enhancement criteria

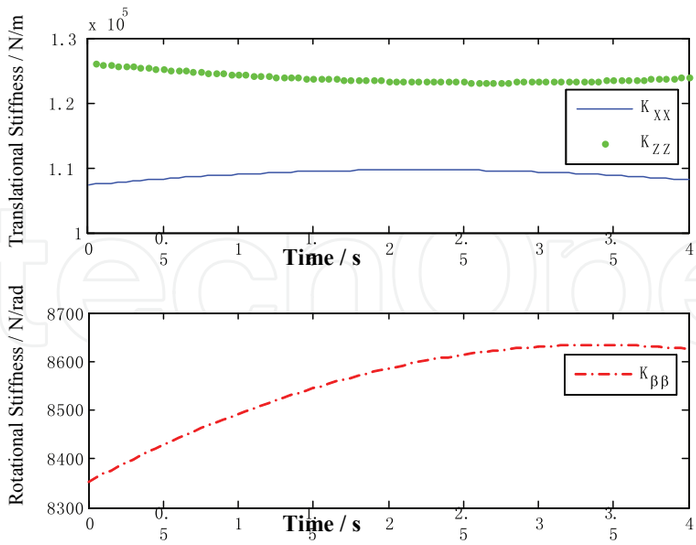

Fig. 5. Stiffness values obtained by the stiffness enhancement criteria

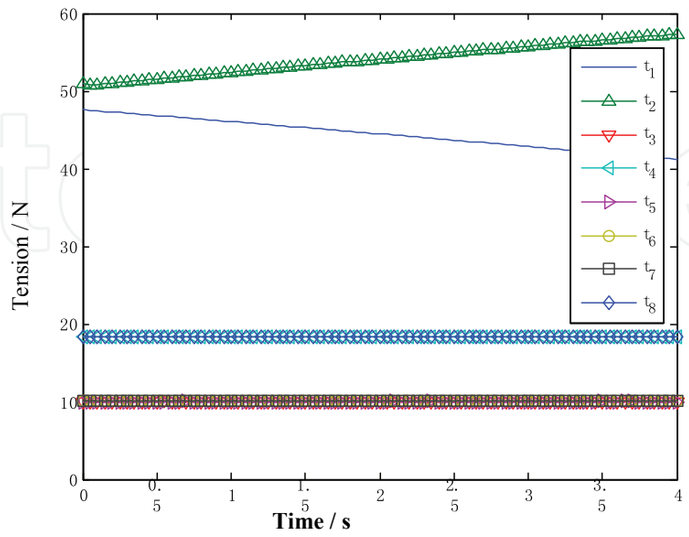

Fig. 6. Optimum tension distribution based on the minimum tension criteria

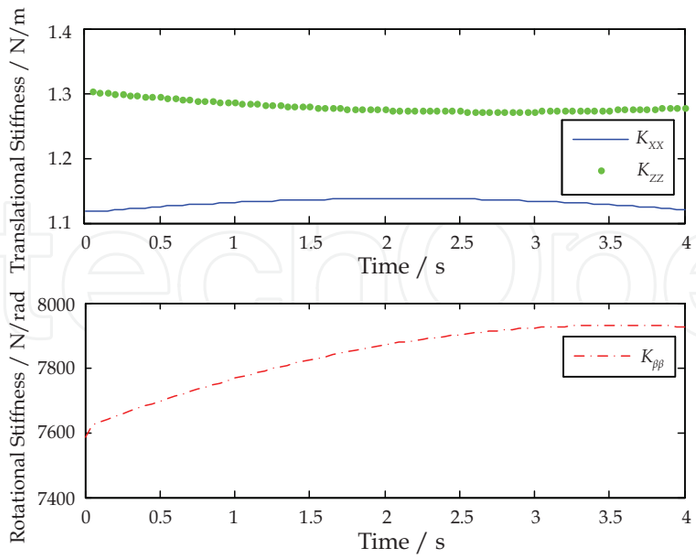

Fig. 7. Stiffness values obtained by the minimum tension criteria

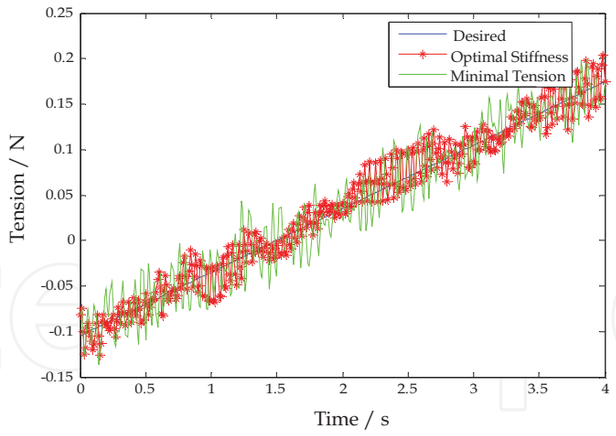

Fig. 8. Pitch angle vs time

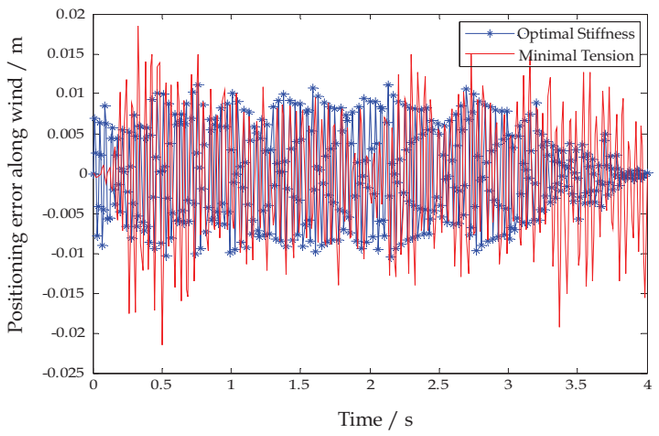

Fig. 9. Position error of the aircraft model at along-wind direction

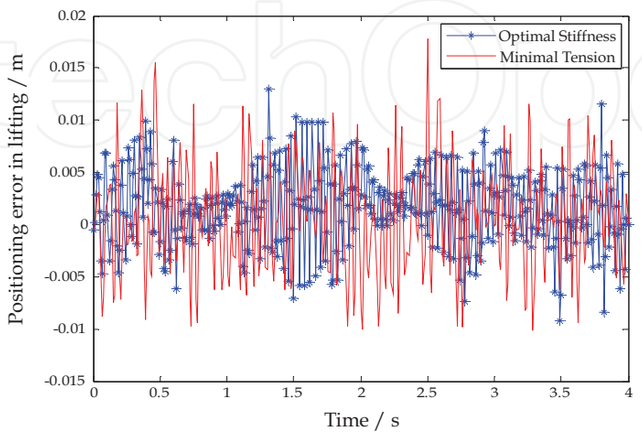

Fig. 10. Pitch angle vs time

7. Conclusions

Firstly, the stiffness of the six-degree-of-freedom redundant wire driven parallel manipulator is dealt with in this paper. The analytical expression of the stiffness is developed, in which the stiffness consists of two parts. The former part is related to the wire tension, while the latter one depends mainly on both the geometry distribution of the wires and the orientation of the end-effector.

Secondly, the dynamical models of the aircraft and the driving system are deduced, respectively. Considering the motor output and wire material properties, the wire tension optimization is conducted in order to improve the stiffness in three principal directions. This method solves the indefinite problem of the wires tension introduced by the redundancy.

Thirdly, aiming at the nonlinearity, strong coupling and air current loaded environment of the wire driven system, the revised PD feed forward controller in joint space based on stiffness enhancement principle is developed. Compared with the revised PD feed forward controller based on minimum wire tension principle, the control scheme proposed in this paper improves the dynamical positioning precision of the aircraft.

8. Acknowledgment

Grateful acknowledgment is made to Prof. Liu Xiongwei and Dr. Zheng Yaqing. The authors would like to appreciate the Editor, Associate Editors, and the reviewers for their valuable comments and suggestions.

9. References

Albus, J.; Bostelman, R. & Dagalakis, N. (1993). The NIST robocrane. *Journal of Robotic Systems*, vol. 10, no. 5, pp. 709-724,

Behzadipour, S. & Khajepour, A. (2006). Stiffness of cable-based parallel manipulators with application to stability analysis. *Journal of Mechanical Design*, vol. 128, no. 1, pp. 303-310.

Chen, Q.; Wang, Y. & Chen, H. (2003). Comparative research of trajectory tracking performance of robotic manipulator based on PD control scheme. *Control and Decision*, vol. 18, no. 1, pp. 53-57.

Dekker, R.; Khajepour, A. & Behzadipour, S. (2006). Design and testing of an ultra-high-speed cable robot. *International Journal of Robotics and Automation*, vol. 21, no. 1, pp. 25-33.

Duan, B.Y. (1999). A new design project of the line feed structure for large spherical radio telescope and its nonlinear dynamic analysis. *Mechatronics*, vol. 9, no. 1, pp. 53-64.

Hithoshi, K.; Toshiaki, Y. & Fumiaki, T. et al. (2007). Robust PD control using adaptive compensation for completely restrained parallel-wire driven robots: translational systems using the minimum number of wires under zero-gravity condition. *IEEE Transactions on Robotics*, vol. 23, no. 4, pp. 803-812, 2007.

Lafourcade, P.; Llibre, M. & Reboulet, C. (2002). Design of a parallel wire-driven manipulator for wind tunnels. *Proceedings of the workshop on Fundamental Issues and Future Research Directions for Parallel Mechanisms and Manipulators*. pp. 187-194. , October 2002,Quebec City, Quebec, Canada,

Lafourcade, P. (2004). Etude de manipulateurs parallel cables, conception d'une suspension active pour souffleria, Dissertation of ENSAE.

Liu, X.; Zheng Y. & Lin, Q. (2004). Overview of wire-driven parallel kinematic manipulators for aircraft wind tunnels. *Acta Aeronautica et Astronautica Sinica*, vol. 25, no. 4, pp. 393-400.

Liu, X. Qi Y. &, Agyemang, B. et al (2006). Design wire-driven parallel suspension system for wind tunnel based virtual flight testing. *Proceedings of the 7th International Conference on Frontiers of Design and Manufacturing*, pp. 7-12, Guangzhou, China, June 2006.

Ma, O. & Diao, X. (2005). Dynamics analysis of a cable-driven parallel manipulator for hardware-in-the-loop dynamic simulation. *Proceedings of the 2005 IEEE/ASME International Conference on Advanced Intelligent Mechatronics.* pp. 837-842 , July 2005, Monterey, California, USA

Ming, A. & Higuchi, T. (1994). Study on multiple degree of freedom positioning mechanisms using wires. Part 1: concept, design and control. *International Journal of the Japan society for Precision Engineering*, vol. 28, no. 2, pp. 131-138.

Müller, A. (2005). Internal preload control of redundantly actuated parallel manipulators-its application to backlash avoiding control. *IEEE Transactions on Robotics*, vol. 21, no. 4, pp. 668-677.

Ning, K.; Zhao, M. & Liu, J. (2006). A new wire-driven three degree-of-freedom parallel manipulator. *Journal of Manufacturing Science and Engineering*, vol. 128, no. 3, pp. 816-819.

Yamamoto, M.; Yanai, N. & Mohri, A. (2004). Trajectory control of incompletely restrained parallel-wire-suspended mechanism based on inverse dynamics. *IEEE Transactions on Robotics*, vol. 20, no. 5, pp. 840-850.

Yu, K. (2008). Simultaneous trajectory tracking and stiffness control of cable driven parallel manipulator. Dissertation of State University of New York.

Zheng, Y. (2004). Research on key theoretical issues of wire-driven parallel kinematic manipulators and the application to wind tunnel support systems. Dissertation of Huaqiao University.

Zheng Y.; Lin, Q. & Liu, X. (2005). Design methodology of wire-driven parallel support systems in the low speed wind tunnels and attitude control scheme of the scale model, *Acta Aeronautica et Astronautica Sinica*, vol. 26, no. 6, pp. 774-778.

Zi, B.; Duan, B. Y. & Du, J. L. et al. (2008). Dynamic modeling and active control of a cable-suspended parallel robot. *Mechatronics*, vol. 18, no. 1, pp. 1-12.

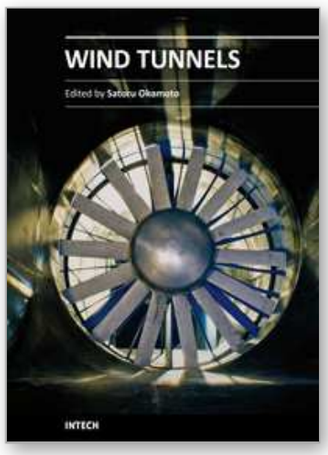

Wind Tunnels

Edited by Prof. Satoru Okamoto

ISBN 978-953-307-295-1

Hard cover, 136 pages

Publisher InTech

Published online 10, February, 2011

Published in print edition February, 2011

Although great advances in computational methods have been made in recent years, wind tunnel tests remain essential for obtaining the full range of data required to guide detailed design decisions for various practical engineering problems. This book collects original and innovative research studies on recent applications in wind tunnel tests, exhibiting various investigation directions and providing a birdâ€™s eye view on this broad subject area. It is composed of seven chapters that have been grouped in two major parts. The first part of the book (chapters 1â€“4) deals with wind tunnel technologies and devices. The second part (chapters 5â€“7) deals with the latest applications of wind tunnel testing. The text is addressed not only to researchers but also to professional engineers, engineering lecturers, and students seeking to gain better understanding of the current status of wind tunnels.ã€€Through its seven chapters, the reader will have an access to a wide range of works related to wind tunnel testing.

InTech Europe
University Campus STeP Ri
Slavka Krautzeka 83/A
51000 Rijeka, Croatia
Phone: +385 (51) 770 447
Fax: +385 (51) 686 166
www.intechopen.com

InTech China
Unit 405, Office Block, Hotel Equatorial Shanghai
No.65, Yan An Road (West), Shanghai, 200040, China
中国上海市延安西路65号上海国际贵都大饭店办公楼405单元
Phone: +86-21-62489820
Fax: +86-21-62489821

IntechOpen